Ecological Applications, 5(3), 1995, pp. 724–739

UPPER OCEAN PHYSICS AS RELEVANT TO ECOSYSTEM DYNAMICS: A TUTORIAL[1]

DAVID ARCHER
Department of the Geophysical Sciences, 5734 South Ellis Avenue, University of Chicago, Chicago, Illinois 60637 USA

Abstract. Oceanic control of the atmospheric carbon dioxide concentration is the link between the studies of plankton ecology and climate change. Modeling ecosystem dynamics requires some understanding of the physics and chemistry of the upper ocean. In addition, an understanding of the issues involved in predicting climate change can help focus ecological studies. This article is intended as a review of upper ocean physics and chemistry as relevant to ecosystem research, and a summary of climate-related issues to which ecosystem dynamics might in the future make a contribution.

Our picture of the carbon cycle in the upper ocean relies on ecosystem dynamics for an understanding of the efficiency of nutrient uptake and export of carbon in the form of sinking carbon particles, and for the fraction of recycled and exported particulate carbon production. A fundamental variable appears to be the size distribution of phytoplankton. Also, ultimately, an understanding of the partitioning between calcitic- and siliceous-based ecosystems may be important to predicting the long-term ocean carbon cycle.

Ecosystem dynamics of the upper ocean are driven by the interplay between dynamics of the surface ocean mixed layer and the depth of light penetration. This interplay is illustrated by noting the effect of high-frequency fluctuations in mixed-layer depth from a physical model (Archer et al. 1993) on an ecosystem model developed at weathership station Papa in the subarctic Pacific ocean (Frost 1987). Three families of surface ocean mixed-layer models are available for use by plankton ecologists, and although the physical mechanisms by which mixing occurs differ among the model groups, all are generally successful at predicting the observed ocean mixed-layer depth. This paper explores behavioral distinctions between the three types of models, and summarizes previously published comparisons of the generality, accuracy, and computational requirements of the three models. Nutrients are supplied to the euphotic zone by the exchange of water between nutrient-depleted surface waters and nutrient-rich deeper waters. Current understanding of this process is still problematic, with rates of mixing required to balance nutrient uptake estimates higher than values predicted based on turbulence studies. I also review evidence that episodic mixing, driven by frontal and mesocale motions, may be responsible for a significant fraction of vertical nutrient transport.

Key words: *CO_2; modeling; ocean carbon cycle, ocean light penetration; pelagic marine plankton; sea surface mixing.*

THE ROLE OF PLANKTON ECOLOGY IN CLIMATE CHANGE RESEARCH

The factors that control the population dynamics of the upper ocean are only poorly understood, and yet they are of some significance to socially crucial issues of climate change. In particular, biological pumping of carbon to the deep ocean maintains a lower concentration of the greenhouse gas CO_2 in the atmosphere than would exist above a "dead" ocean. Certain very specific changes in the biological pump could drive large changes in atmospheric CO_2, in particular changes in nutrient utilization efficiency in the high-latitude oceans (Knox and McElroy 1984, Sarmiento and Toggweiler 1984, Siegenthaler and Wenk 1984), or changes in the balance between calcitic and siliceous communities (Archer and Maier-Reimer 1994). The size distribution of phytoplankton appears to be a major controller of recycling efficiency and carbon export from the surface ocean. At the same time, ocean ecologists must take care to avoid making excessive claims about the ability of biological processes to sequester fossil fuel CO_2 (Broecker 1991).

The biological pump and seawater carbonate chemistry

Biological production in the surface ocean produces particles that sink into deeper waters, where they for the most part redissolve. This process (called the "biological pump") maintains lower concentrations of carbon and nutrients in the surface ocean than within the thermocline waters below. Removal of dissolved CO_2 to form organic matter lowers the steady-state sea surface pCO_2 (partial pressure of CO_2; see *Aqueous chemistry*, below) relative to an abiotic ocean. Less important quantitatively is the removal of dissolved $CO_3^=$ to

[1] Manuscript received 5 November 1993; revised 12 October 1994; accepted 13 October 1994; final version received 29 November 1994.

form solid $CaCO_3$ (the minerals calcite and aragonite), which tends to increase pCO_2.

A summary of carbonate buffer-system chemistry.—The counter-intuitive inverse behavior between CO_2 and $CO_3^=$ is the result of the carbonate buffer system in seawater, which can be summarized as follows. Atmospheric CO_2 dissolves in seawater and is hydrated to form carbonic acid, H_2CO_3. Carbonic acid is divalent; that is, it can undergo two de-protonation reactions to form bicarbonate (HCO_3^-), and carbonate ($CO_3^=$). The coexistence of these species in seawater creates a chemical buffer system, regulating the pH and the pCO_2 of the oceans. Most of the inorganic carbon in the ocean exists as bicarbonate (≈88%), with the concentrations of carbonate ion and CO_2 comprising ≈11% and 1%, respectively. (A standard text for this topic is Stumm and Morgan 1981.)

Aqueous chemistry.—The hydration reaction of CO_2 to form H_2CO_3 is described by the following equilibrium system:

$$H_2CO_3 = CO_2 + H_2O,$$

$$K = \frac{\{CO_2\}_{aq}}{\{H_2CO_3\}}, \quad (1)$$

where K is a thermodynamic equilibrium constant. A thermodynamic equilibrium constant is defined in terms of species activities, as above.

Notation Convention

The *activity* of a solute represents the apparent concentration, which approaches the actual concentration near the limit of infinite dilution. In this paper, braces, e.g., $\{CO_2\}$, denote activity; brackets, e.g., $[CO_2]$, denote concentrations.

Analytical determination of the relative activities of H_2CO_3 and CO_2 is difficult, so it is convenient to group the two species together using the notation:

$$H_2CO_3^* = H_2CO_3 + CO_2. \quad (2)$$

Carbonic acid undergoes de-protonation to form bicarbonate and carbonate ion. The equilibrium expression for the first pH reaction is expressed using the $H_2CO_3^*$ notation (this is called a *composite* equilibrium expression):

$$H_2CO_3^* = H^+ + HCO_3^-,$$

$$K_1 = \frac{\{H^+\}\{HCO_3^-\}}{\{H_2CO_3^*\}}. \quad (3)$$

The second dissociation reaction is described by

$$HCO_3^- = H^+ + CO_3^=,$$

$$K_2 = \frac{\{H^+\}\{CO_3^=\}}{\{HCO_3^-\}}. \quad (4)$$

For convenience, apparent equilibrium constants, denoted by primes, can be defined in terms of concentrations of the carbonate species, rather than activities, as

$$K'_1 = \frac{\{H^+\}[HCO_3^-]}{[H_2CO_3^*]},$$

$$K'_2 = \frac{\{H^+\}[CO_3^=]}{[HCO_3^-]}. \quad (5)$$

Numerous authors have published values for K'_1 and K'_2, (Hansson 1973, Mehrbach et al. 1973, Dickson and Millero 1987, Roy et al. 1993), and the selection of the best pair is still a matter for research and debate (Millero et al. 1993, T Takahashi, D. Archer and D. Chipman, *unpublished manuscript*). One set of expressions for K'_1 and K'_2 is given in the Appendix: Part A.

The interaction between the carbonate species in seawater leads to the aforementioned counter-intuitive inverse behavior between CO_2 and $CO_3^=$. When carbonate ion is removed from solution (such as by formation of solid $CaCO_3$), bicarbonate ion undergoes a disproportionation reaction (until the equilibrium expressions (Eq. 5) are satisfied):

$$2\ HCO_3^- \rightarrow H_2CO_3 + CO_3^=. \quad (6)$$

The net result of this transaction is to increase the pCO_2 of the water parcel as $CO_3^=$ is removed. (Contrast this with the simple-minded expectation that removal of a carbon species ($CO_3^=$) should reduce the concentrations of all other carbon species, the "falling tide lowers all boats" scenario). Natural variations in seawater pH cause the relative concentrations of CO_2 and $CO_3^=$ to vary inversely with each other, like the seats on a teeter-totter, while the relative changes in the concentration of HCO_3^- are much smaller.

The carbonate buffer system as written above has two degrees of freedom; that is, two measurements are required to specify the system entirely. The "alkalinity" of a sample is defined as the amount of acid required to neutralize all of the weak bases in the solution (primarily bicarbonate and carbonate ion), and can be measured by pH titration (see Stumm and Morgan 1981). Other practical measurements include the concentration of ΣCO_2 (defined as $CO_2 + HCO_3^- + CO_3^=$; measurement technique by Johnson et al. 1985), and the pCO_2 (Chipman et al. 1992), and pH (Clayton and Byrne 1993). Measuring pCO_2 directly is the most reliable way of determining air-sea pCO_2 differences in the field. However, for modeling CO_2 in the ocean, pCO_2 should be calculated from the alkalinity and ΣCO_2, since these are conservative to mixing. A simple algorithm for calculating pCO_2 from alk and ΣCO_2 is given in the Appendix: Part B.

Gas equilibrium chemistry.—The equilibrium partitioning of CO_2 between atmospheric and dissolved states is described by Henry's law:

$$K'_H = \frac{pCO_2}{[CO_2]}, \quad (7)$$

where K'_H is called the Henry's law constant. The inverse of the Henry's law constant is referred to as K'_0. The pCO_2, or "partial pressure" of CO_2, is defined as the gas pressure exerted by CO_2 in the head space above a water sample at equilibrium. Seawater that is not in gas-exchange equilibrium with the atmosphere will have a pCO_2 that is different from the atmospheric value.

The Henry's law coefficient, K'_H, varies strongly with temperature, tending to higher pCO_2 at higher temperature. The $[CO_2]_{aq}$ is also affected by the temperature dependence of K'_1 and K'_2 (for a full treatment of these effects, see Broecker and Peng [1982]: 150). The net temperature dependence of seawater pCO_2 is an increase by ≈4.23% per degree Celsius (Takahashi et al. 1993).

The pCO_2 of sea water is buffered by the carbonate system, relative to a non-pH-active gas like O_2. This is because a change in pCO_2 must be accompanied by changes in the concentrations of bicarbonate and carbonate ions. At the normal pH of seawater, the carbonate buffer system provides an effective reservoir for CO_2 that is roughly 10 times larger than the reservoir for an unbuffered gas like O_2. Therefore, the equilibration time of seawater pCO_2 is roughly 10 times slower than that for O_2. The "buffering strength" of seawater is often expressed as the Revelle buffer factor (γ), which is defined as the ratio between the relative sensitivity of pCO_2 and total CO_2 to an incremental addition or removal of CO_2 to a water parcel:

$$\gamma = K'_H = \frac{\partial pCO_2/pCO_2}{\partial TCO_2/\Sigma CO_2} = \frac{\partial \ln pCO_2}{\partial \ln TCO_2}.$$

For example, the average value of γ in global ocean surface waters is about 10. Therefore, a 1% increase in ΣCO_2, about 20 μmol/kg in typical surface seawater with ΣCO_2 = 2000 μmol/kg, will result in an increase in pCO_2 of 10%, which corresponds to an increase in H_2CO_3* of ≈2 μmol/kg. The numerical correspondence between the factor-of-10 decrease in gas equilibration response time described above and the value of the Revelle buffer factor of approximately 10 is merely a confusing coincidence. Waters with a smaller value of the Revelle factor γ can take up more CO_2. Global surface ocean waters range from γ = 8 in low-CO_2 tropical surface waters to γ = 12 in high-CO_2 polar waters, and in deep water containing high CO_2 concentrations γ can reach as high as 17 (Takahashi et al. 1980, 1993).

Nutrient limitation and the high-nutrient low-productivity (HNLP) problem

Biological uptake of carbon is limited by the availability of the dissolved macronutrients NO_3 and PO_4. The elemental composition of "generic marine organic matter" was estimated by Redfield (1934) to be C : N : P : O_2 = 106:16:1:−138, and revised by Takahashi et al. (1985) to be 103:16:1:−172. In either case, the availability of nutrients provides a strong constraint on the ability of the biota to export carbon to the deep sea. Because of this limitation, the biological pump in a high-CO_2 climate should be to first order about as strong as it is today; that is, the biological pump is not likely to sequester fossil fuel CO_2 (Broecker 1991) unless there is some change either in nutrient availability (by either a change in circulation or by sources of anthropogenic nutrients; Owens et al. 1992) or in the efficiency of nutrient uptake by plankton under conditions of higher CO_2 (Riebesell et al. 1993). The biological pump could even be weakened under conditions of high ultraviolet (UV) radiation fluxes resulting from an ozone-depleted atmosphere if UV adversely affects phytoplankton (Smith et al. 1992; Holm-Hansen et al. 1993).

In many regions of the world's oceans (the North Pacific, the Southern Ocean, and the equatorial Pacific) surface biomass production does not fully deplete the surface nutrients during the summer growing season. In these regions, higher efficiency of nutrient utilization (i.e., lower nutrient concentrations) could drive sea-surface pCO_2 to lower values. Simple box models of the ocean–atmosphere system have shown that the atmospheric pCO_2 is particularly sensitive to nutrient concentration in the high-latitude oceans (Knox and McElroy 1984, Sarmiento and Toggweiler 1984, Siegenthaler and Wenk 1984). If nutrients in the high-latitude surface waters were completely utilized by primary production, then the pre-industrial atmospheric volumetric mixing ratio of CO_2 (volume of CO_2 per total volume) could have been as low as 165 μL/L (ppm); the lower efficiency of nutrient use could have increased the mixing ratio to as high as 425 μL/L (pre-industrial atmospheric pCO_2 was 280 μL/L). Obviously, understanding the factors limiting growth in these regions, and predicting how they might respond to changing climate, is crucial to global CO_2 modeling. Unfortunately, the limitation of phytoplankton growth is still a subject of research and debate.

One hypothesis is that the rate of primary production is limited by grazing by microzooplankton (Evans and Parslow 1985, Frost 1987, Fenchel 1988). Microzooplankton have short reproductive cycles, and so can respond quickly to variations in primary production, in contrast to macrozooplankton, which have annual reproductive cycles. In the North Atlantic, where the spring bloom depletes the surface nutrients, it could be that the phytoplankton escape predation in the spring because of the deeper wintertime mixed layer (which depletes microzooplankton stocks to low levels (Frost 1987)).

Another hypothesis involves the micronutrient iron, which may be limiting the primary production rate in some regions (Martin and Fitzwater 1988, Martin and

Gordon 1988). Iron is thought to be used by phytoplankton in the enzymatic system for conversion of nitrate to ammonia; thus, a limitation of iron would inhibit new (nitrate-based) growth (Reuter and Ades 1987, Morel et al. 1991). Growth experiments using phytoplankton samples from the North Pacific were performed by Martin and Fitzwater (1988) both with and without the addition of trace quantities of iron, and in most cases the iron-added system showed enhanced phytoplankton growth rates relative to the low-Fe control. Iron is supplied to the surface ocean by atmospheric flux of continental dust (Martin and Fitzwater 1988), and regions of low nutrient utilization tend to correspond to regions of low atmospheric particulate input.

Recent work in the subarctic Pacific (the Subarctic Pacific Ecosystem Research program) has generated what has become known as the "SUPER synthesis" of these two hypotheses (Miller et al. 1991). The growth rates of small phytoplankton appear to be unlimited by the availability of iron; that is, in in situ conditions the doubling time of picophytoplankton approaches physiological limits. However, production of picoplankton is limited by microbial grazing (Frost 1987). When iron is added to these waters, after a few days nutrient uptake becomes dominated by large diatoms (Martin and Fitzwater 1988), which are able to escape predation and bloom to the limit of available macronutrients. Thus, understanding the factors that control phytoplankton size appears to be of fundamental importance to a predictive understanding of the HNLP phenomenon. The efficiency of nutrient recycling must also be closely controlled by plankton size, with lower efficiency in systems dominated by larger grazers that produce quickly sinking fecal material, relative to the slow sinking velocity of microbial grazer fecal material. In addition, the potential for fish production is also fundamentally limited by the size characteristics of organisms at the bottom of the food chain (Ryther 1969). Thus a predictive model for the size distribution of plankton as a function of environmental conditions would be extremely useful to prediction of air–sea carbon fluxes, nutrient utilization efficiency, new vs. recycle production, and fisheries yields.

Partitioning between calcitic and siliceous ecosystems

Much of the interdisciplinary research between the fields of chemical and biological oceanography has concentrated on elucidating the factors that control the export of organic carbon to the deep sea. The next step must be the prediction of the functional groups of plankton. According to recent ideas about the carbon cycle in the ocean, the relative production rates of calcite and organic carbon can have a significant impact on the pH of the ocean and the pCO_2 of the atmosphere (Archer and Maier-Reimer 1994). The proposed sensitivity of atmospheric pCO_2 to calcite production led to the speculation that lower rates of calcite production, and higher rates of organic carbon production, during the last glacial maximum could account for lower pCO_2 at that time. The balance between organic carbon and calcite could most easily be perturbed by shifting globally from calcitic (coccolithophorid) production toward siliceous (diatom)-based ecosystems. Factors that seem to control calcitic vs. siliceous ecosystems include temperature and dissolved silicate (Lisitzin 1967). However, the details of this remain obscure, and prediction of the calcite/silicate ecosystem response of the upper ocean to changes in climate and ocean circulation are still beyond our grasp.

In addition to their alleged long-term effect on atmospheric CO_2, the functional characteristics of phytoplankton production can also be significant to trace gases such as dimethyl sulfide, produced by coccolithophorids (Keller et al. 1989). Dimethyl sulfide production is one of the major terms in the natural sulfur cycle of the atmosphere, and has been implicated in the formation of cloud condensation nuclei (Charlson et al. 1987).

The Role of Upper-Ocean Physics in Plankton Ecosystem Modeling

Given that ecosystem dynamics have some part to play in understanding the carbon system of the upper ocean, I now make the case that the physics of mixing and light transmission appear to be primary drivers to the ecosystem dynamics of the upper ocean. The depth of surface momentum and buoyance flux-driven mixing are predictable using available physical models, if meteorological conditions at the sea surface are known. However, the physics of mixing of nutrients across the stratification of the upper ocean are not well understood, and may currently present the ecosystem modeling community with some difficulty.

The depth of turbulent mixing and light penetration

Phytoplankton photosynthesis is fundamentally controlled by the depth of turbulent mixing at the ocean surface coupled to the depth of sunlight penetration (the "euphotic zone"). The mixing time of waters in the mixed layer is fast relative to the time scale of plankton motility or population response. This means that when the mixed-layer depth is deeper than some critical depth (called the "Sverdrup depth"), the rate of photosynthesis is light limited. In spring, when thermal stratification drives shoaling of the mixed layer to shallower depths than the critical depth, the "spring bloom" is triggered (Sverdrup 1953).

I illustrate the impact of mixed-layer depth fluctuations on plankton population dynamics using a high-resolution one-dimensional coupled physics–ecosystem model of the mixed layer from weathership station Papa in the subarctic Pacific. The physical simulation was described by Archer et al. (1993), and compared

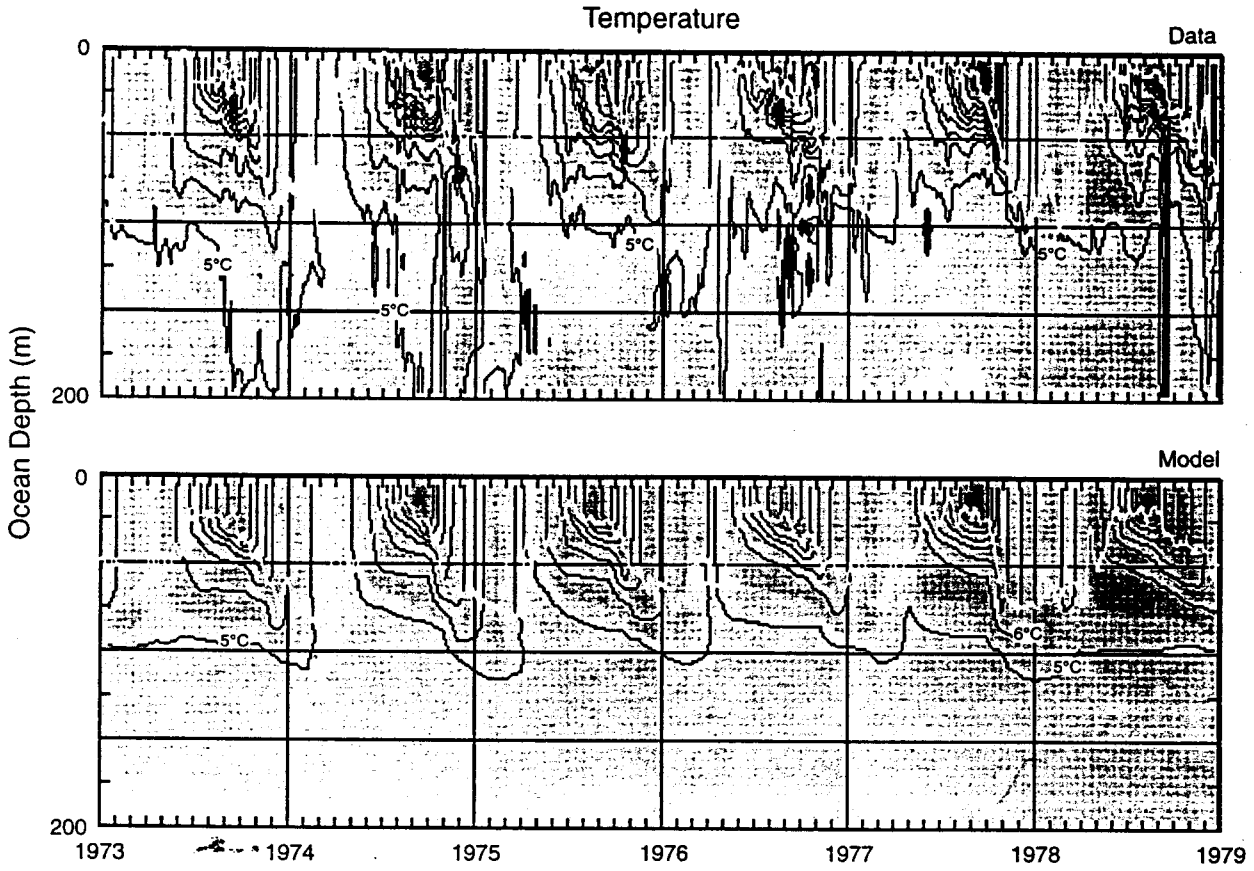

FIG. 1. Near-surface temperature cycles from weathership station Papa in the north Pacific ocean (140° W, 50° N), comparison of data and model results. The continuous white lines indicate the depth of the mixed layer; black lines are contours at intervals of 1° C. Reprinted from Archer et al. (1993).

with observations from the Canadian Weathership Program during the years 1973–1978. Model temperature structure is compared with observations in Fig. 1. The biological ecosystem model was developed as part of the Subarctic Pacific Ecosystem Research program (Frost 1987, Miller et al. 1991). The ecosystem model was run off-line; i.e., daily values of mixed-layer depths and sea surface temperatures from the model, and sunlight intensity data from the weathership, were used to drive the ecosystem model. The parameters in the ecosystem model are appropriate to conditions of relatively low mixed-layer depth variability (Frost 1987), and the response of the model most resembles data from weathership station Papa in the low-variability simulations.

Springtime warming drives shoaling of the mixed layer, which confines phytoplankton to the well-lit depth near the surface. Thus, fluctuations in mixed-layer depth drive variability in the chlorophyll concentration of the model (Fig. 2). When the model mixed-layer depths are sub-sampled on longer time intervals, the variability of the chlorophyll concentration decreases (Fig. 3). This example illustrates how upper ocean mixing dynamics can drive the behavior of the planktonic ecosystem, and motivates the coupling of ecosystem dynamics models with models of physical mixing. The next section explains the inputs required by mixing models, and reviews the existing literature on the physics of mixing in the upper ocean.

Air–sea fluxes

Mixed-layer models, such as the one used above, are driven by air–sea fluxes of heat and fresh water (which determine the "flux" of water density, or buoyancy), and momentum.

Heat.—Heat is transferred between the surface ocean and the atmosphere by the mechanisms of evaporation (latent heat flux), radiation (both direct short-wave sunlight and net long-wave radiation), and conduction (the sensible heat flux). In most cases, the incoming short-wave radiation and outgoing evaporative heat dominate. The oceans transport heat from low latitudes to high latitudes, so that in low latitudes, downward heat transport exceeds local upward heat transport. Thus, only in mid-latitudes can the heat fluxes be expected to balance locally (Peixoto and Oort 1992).

The "bulk" formulas for sensible (H) and latent (L_vE) heat fluxes involve the density of air (ρ_{air}), drag (transfer) coefficients (C_H for latent and C_E for evaporative), the wind speed at a height of 10 m (U_{10}), and

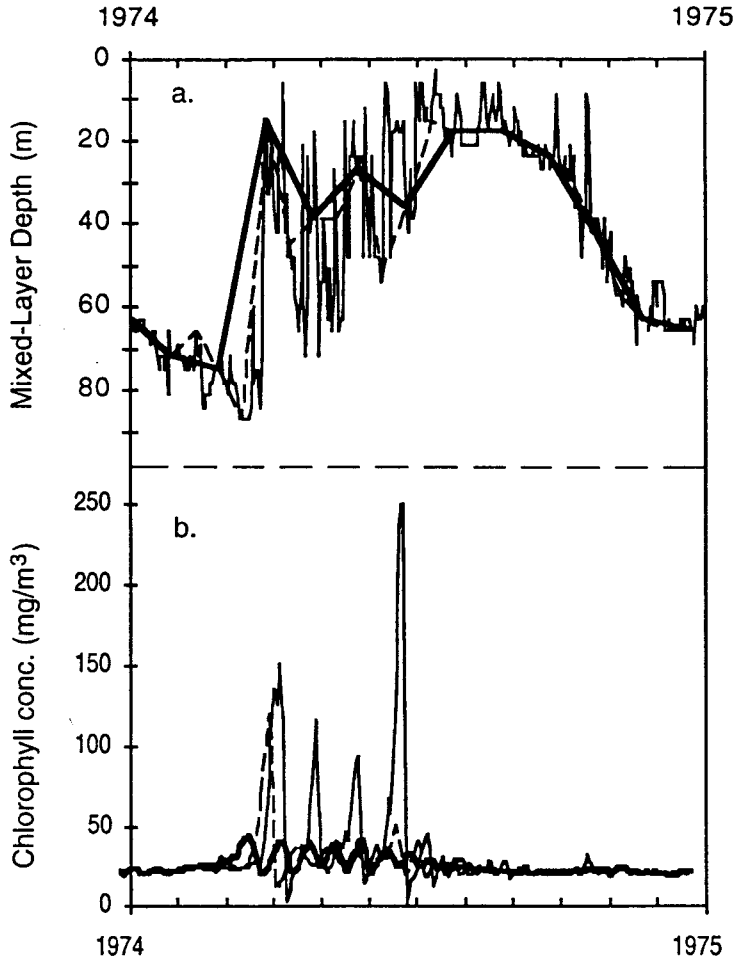

FIG. 2. (a) Time series of mixed-layer depth from the Papa model, daily values (solid line), and subsampled on intervals of 15 d (dashed line) and 30 d (heavy line). (b) Ecosystem model chlorophyll concentration using the model mixed-layer depths from the curves in (a). As mixed-layer depth fluctuations are eliminated by subsampling the physical model output, the short-term fluctuations of chlorophyll in the ecosystem model diminish.

the difference in temperature (T, where the subscript "s" denotes water surface, and "a" denotes air) or water saturation (relative humidity, RH), respectively (from Gill 1982):

$$H = \rho_{air} c_p C_H U_{10} (T_s - T_a) \quad (8)$$

and

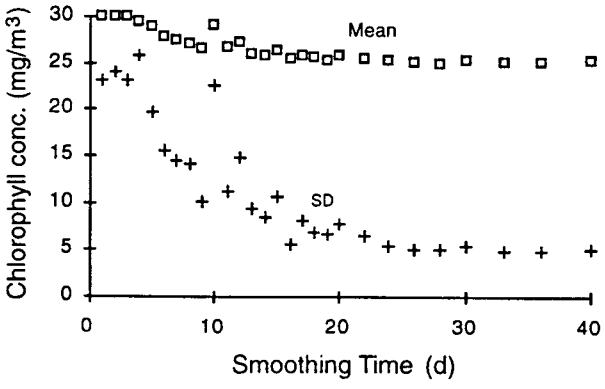

FIG. 3. Mean and variance (1 SD) of model chlorophyll from Fig. 2, plotted as a function of subsampling time. Mean values decrease somewhat, and variance diminishes rapidly, as mixed-layer depth fluctuations are removed.

$$L_v E = \rho_{air} L_v C_E U_{10} (RH_s - RH_a). \quad (9)$$

The best value for C_H ranges from 0.85×10^{-3} (stable atmospheric conditions) to 1.10×10^{-3} (unstable conditions). C_E is estimated to be 1.5×10^{-3}.

The formulation for the heat flux caused by radiative transfer is somewhat more complicated. The input radiation ($Q_{I,0}$) can be described as a function of latitude and season (Frouin et al. 1989). Some of the incoming radiation is blocked by clouds in the atmosphere. The effect of clouds represents a major uncertainty in the heat balance of the surface ocean (Seager et al. 1988, Wigley 1989, Mitchell et al. 1989). In addition to oceanic heat gain by incoming light, some heat is lost by outgoing blackbody radiation. There exist several formulations to calculate the net radiative heat flux; the following was presented by Gill (1982):

$$Q_I = Q_{I,0}(1 - \alpha_s)(1 - 0.7n_c) \quad (10)$$

and

$$Q_B = 0.985\sigma T_s^4 (0.39 - 0.05 e_a^{1/2})(1 - 0.6 n_c^2), \quad (11)$$

where Q_I is the downward radiative heat flux, $Q_{I,0}$ is the value at the top of the atmosphere, Q_B is the upward long-wave radiation, α_s is the surface albedo (roughly

0.3), n_c is the fractional cloud cover, σ is the Boltzmann constant, T_s is the sea surface temperature, and e_a is the vapor pressure of the atmosphere (in mbar). The standard deviation of the uncertainty of the total heat flux has been estimated to be on the order of 25 W/m^2 (Weare et al. 1981; see also Davis et al. 1981, Seager et al. 1988). For comparison, the global average heat flux is on the order of 240 W/m^2 (Gill 1982), and the perturbation due to the anthropogenic CO_2 will be $\approx$4 W/m^2 (Lorius et al. 1991).

Fresh water.—The net flux of fresh water across the air–sea interface is determined by the difference between evaporation and precipitation. A bulk formula for the evaporation flux was given above (Eq. 9). Atlases of precipitation rate are available from Peixoto and Oort (1983) and Baumgartner and Reichel (1975), but in general the uncertainties are quite large (for example, see Archer et al. 1993).

Light.—The vertical distribution of photosynthesis is determined by the penetration of light into the upper ocean and by the depth profile of nutrients. Light penetration (as opposed to absorption at the surface) may also have an effect on the sea surface temperature (Woods and Barkmann 1986). Ocean waters have been divided into three optical types (Jerlov 1976) according to the optical characteristics of their suspended particulate material. In the open ocean the concentration of suspended detritus is low, and the optical properties are largely regulated by the abundance of phytoplankton chlorophyll. If we treat the light field as has having only two components, then we can approximate the profile of light energy with depth as:

$$Q(z) = Q_{\text{blue},l} e^{-k'z} \tag{12}$$

and

$$k' = 0.04 + 0.0088\text{Chl} + 0.054\text{Chl}^{2/3}, \tag{13}$$

where z is the depth in metres in the ocean, $Q_{\text{blue},l}$ is the incidence of the blue visible light at the sea surface (roughly half of the total radiative energy), and Chl is the concentration of chlorophyll (from Parsons et al. 1984). Only the blue, penetrating fraction of the light is photosynthetically active radiation (PAR). The rest of the light energy ($Q_{\text{red},l}$) is red light, which is absorbed in the top metre. State-of-the-art models of PAR and light energy input to the mixed layer include such factors as wavelength-dependent absorption, latitude, season, and angle of solar input (Morel 1988, Sathyendranath and Platt 1988).

Momentum.—The wind stress on the ocean surface can be calculated from the square of the wind speed at a height of 10 m (U_{10}), the density of air (ρ_{air}), and a drag coefficient (C_D) (from Wu 1982):

$$\tau = \rho_{air} C_D U_{10}^2. \tag{14}$$

The drag coefficient, C_D is often represented by a constant. However, the high seas that result from heavy winds tend to increase C_D. Values of the drag coefficient as a function of wind speed were summarized by Wu (1982):

$$C_{10} = 10^{-3}(0.8 \pm 0.065U_{10}). \tag{15}$$

When this expression is incorporated into Eq. 7, the momentum flux into the surface layer scales as the wind speed to the third power. Since the momentum flux is a nonlinear function of the wind speed, the use of wind speeds averaged over time scales of weeks to months results in underestimation of wind-driven mixing (for example, see Rosati and Miyakoda 1988).

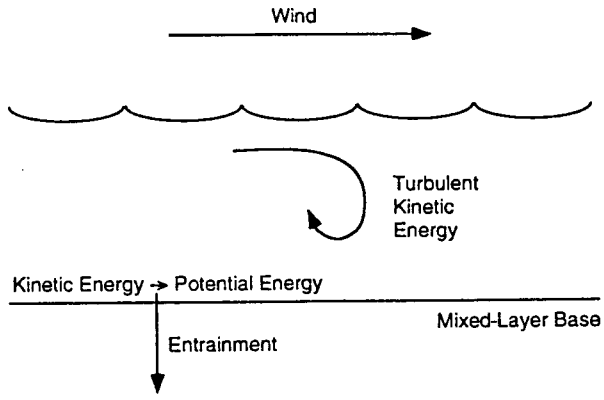

FIG. 4. Diagram of the "integrated turbulent kinetic energy" models. "→" denotes where the kinetic energy of currents turns into the potential energy of mixing against stratification.

Mixing models

Given the inputs of heat, fresh water, and momentum from the atmosphere, a one-dimensional mixed-layer model predicts the depth of the mixed layer, and, in some models, the shape of the mixed-layer base, as a function of time. There are three basic families of mixed-layer models: the "bulk turbulent kinetic energy (TKE)" models, the "shear instability" models, and the "turbulence closure" models (see Niiler and Kraus 1977, Martin 1985, 1986). The assumed physical mechanisms by which entrainment occurs differ fundamentally among the three families, but all are reasonably successful at predicting the observed depth of the mixed layer.

Integrated TKE, or "bulk", models.—The so-called bulk turbulent kinetic energy (TKE) model, initially formulated by Kraus and Turner (1967), treats mixing based on a budget for the integrated TKE of the surface ocean (Fig. 4). A fundamental assumption of this model is that the mixed layer is completely homogeneous in the various state variables (temperature, T; salinity, S; currents; TKE; solutes; etc.). This assumption appears to be well founded in most parts of the surface ocean (see Martin 1986, Price et al. 1986). A heat balance is constructed that accounts for exchange with the atmosphere (L,E and H, Eqs. 8 and 9) and fluxes by radiative transfer (Q_l, Eqs. 10 and 11), and cooling

caused by entrainment of colder water from below (as the mixed-layer depth, h, changes with time):

$$h\frac{dT_s}{dt} = \Lambda\frac{dh}{dt}\Delta T - \frac{1}{\rho_{sw}c_p}(Q_I - Q_{blue,I}e^{-k'z} - Q_B - L_vE - H), \quad (16)$$

where

$$\Lambda = 0 \text{ if } \frac{dh}{dt} < 0$$

amd

$$\Lambda = 1 \text{ if } \frac{dh}{dt} > 0.$$

T_s is the sea surface temperature, and ΔT is the temperature difference across the mixed-layer base; ρ_{sw} is the density of sea water; c_p is the heat capacity of seawater.

The two degrees of freedom in Eq. 16 are the sea surface temperature and the depth of the mixed layer; another independent equation is necessary to close the system. The requisite constraint is based on a kinetic energy budget. The source of TKE is the wind stress (a scaling coefficient, m, times the "friction velocity" of the wind, U^{*3} [U^{*3} is defined as the square root of the surface wind stress τ divided by ρ_{air}]) and the sink is dissipation, D. The residual kinetic energy (the difference between input and dissipation) is transformed into potential energy by mechanical mixing of cold water into the mixed layer (also, the average TKE of the mixed layer decreases as quieter water is entrained):

$$\frac{1}{2}\frac{dT_s}{dt}h^2 + \Lambda\Delta T h\frac{dh}{dt} = mU^{*3} - D. \quad (17)$$

Since Kraus and Turner (1967), many other workers have used models based on this formulation, and much of the work has centered on the dissipation of turbulence (see Stevenson [1979] for a review). The generation and dissipation of turbulence is the greatest weakness of this type of model; in the case of dissipation in particular, the link between the model and the actual physics is weak. Some authors scale TKE dissipation as a constant loss rate times the mixed-layer depth (Kim 1976, Niiler and Kraus 1977). Others calculate the dissipation rate as a function of the total amount of mixed-layer TKE, the coriolis parameter (Garwood 1977) and/or the Monin-Obukhov length scale for turbulence (Gaspar 1988). To simulate the mixed-layer response to hurricanes, Elsberry et al. (1976) used a parameterization for dissipation as a fraction of surface input of TKE that increases with increasing mixed-layer depth.

The other weakness of the bulk TKE family of models is the generation of TKE, calculated as a constant, m, times the wind stress. The value of m is "tuned" to fit the model predictions to observed data, and the best value for the m tends to vary with location and conditions (ranging from 0.1 to 0.39, Martin 1985; 0.3 to 0.9, Price et al. 1978; and 0.4 to 0.5, Davis et al., 1981). The instability of m and the uncertainty about TKE dissipation certainly detract from the predictive ability of the bulk TKE-type model.

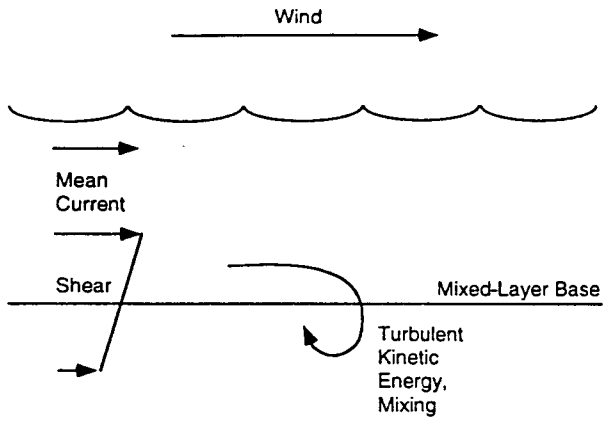

FIG. 5. Diagram of the "shear instability" models. "→" as in Fig. 4.

Shear instability models.—Another potential source of TKE, not considered in the original Kraus-Turner formulation, is the generation of turbulence by current shear (Fig. 5). Although the only source of energy to the mixed layer is input by wind, in the shear models this energy is assumed to generate mean flow rather than turbulent energy, and the flow is converted to turbulence at the base of the mixed layer (see Gargett et al. 1979).

Formulation.—Mixing in a stratified fluid is governed by the gradient of velocity with depth (shear) and the density stratification (Ellison and Turner 1959). The relevant nondimensional parameter is calculated as the ratio of these quantities (from Price et al. 1986).

$$\mathrm{Ri}_{gr} = \frac{g\dfrac{\partial\rho}{\partial z}}{\rho_{sw}\left(\dfrac{\partial u}{\partial z}\right)^2}, \quad (18)$$

where g = the force of gravity, ρ_{sw} = seawater density with depth (z), and u = current velocity; it is called the gradient Richardson number, Ri_{gr}.

The Richardson number used in most mixed-layer models is defined somewhat differently. The mixed layer is viewed as a slab, with uniform velocity and density. Instead of the differential quantities $\partial p/\partial z$ and $\partial u/\partial z$, the differences $\Delta p/h$ and $\Delta u/h$ are used, where Δp and Δu are the changes in density and velocity across the mixed-layer base. The length scale is the thickness of the mixed layer, h, rather than a scale associated with the thickness of the mixed-layer base. The dimensionless number thus defined,

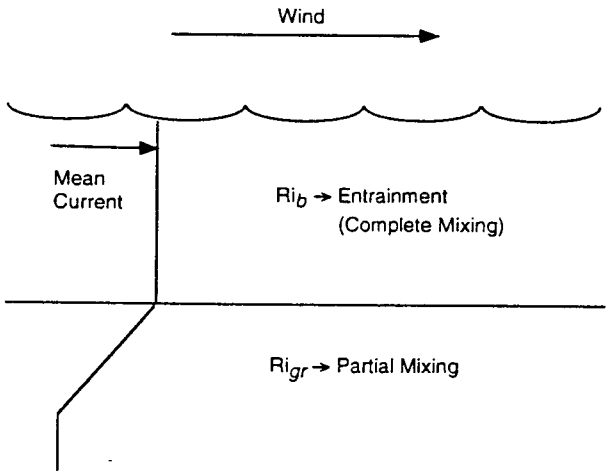

FIG. 6. Diagram of the Price et al. (1986) shear instability model.

$$Ri_b = \frac{g\Delta\rho h}{\rho_{sw}(\Delta)^2}, \quad (19)$$

is called the "bulk Richardson number" (Pollard et al. 1973, Price et al. 1986). In the shear models, mixing is assumed to begin when Ri_b falls below a critical value, and water is entrained until Ri_b reaches the critical value once again. Models based on the bulk Richardson number predict mixed-layer variations quite well, and the only potentially "tunable" parameter is the critical Richardson number, which appears to be stable throughout a variety of locations and climatic conditions (Price et al. 1978, 1986). Theoretical justification for use of the bulk, rather than the gradient, Richardson number for these models is still a matter of discussion (Pollard et al. 1973, Price et al. 1978).

The shear instability model of Price et al. (1986) uses both Ri_b and Ri_{gr} to determine mixing (Fig. 6). The model was used to simulate detailed diurnal fluctuations in the mixed-layer depth and current profiles from the subtropical Pacific. In the model the heat fluxes (except penetrating solar radiation) and the wind stress are applied to the mixed layer. The bulk Richardson number at the base of the surface box is calculated, and if the shear is greater than the density stratification necessary to support it ($Ri_b < 0.65$), then the properties of the two adjacent boxes are averaged (the boxes are mixed). This process continues downward until $Ri_b > 0.65$. The mixed layer is considered homogeneous for momentum and density, as it is in the bulk TKE formulations considered above. The density transition at the mixed-layer base is smoothed using the gradient Richardson number. If Ri_{gr} between two adjacent boxes is smaller than a critical value ($Ri_{gr} < 0.25$), the adjacent boxes are partially mixed until the shear becomes subcritical again, and the process is repeated until Ri_{gr} is greater than or equal to the critical value throughout the water column. Thus, there is a region of partial mixing below the completely mixed zone. The model also incudes convective entrainment driven by surface cooling.

Behavior.—A model in which the generation of turbulence scales with the Richardson number behaves differently from a model that scales turbulence directly with wind stress (Price et al. 1978). This is largely because of the rotation of an inertial current relative to the surface of the earth (the coriolis effect). In the presence of steady, non-rotating wind forcing, a natural limit is imposed on the current velocity by the "inertial" rotational frequency (the value for which varies as a function of latitude). The advantage of scaling entrainment to the current velocity, as opposed to scaling with the wind stress directly, is that the current velocity is limited by the rotational frequency, and no artificial dissipation term is required to limit the steady-state mixed-layer depth. (With constant wind forcing and no dissipation term, a TKE model would entrain forever). As we have seen the treatment of dissipation is one of the major weaknesses in the TKE model formulation.

Also, the value of the critical Ri_b required to simulate oceanographic data using a shear instability mixed-layer model is fairly constant throughout a range of climatic conditions (Pollard et al. 1973, Price et al. 1978, 1986). This can be contrasted with the wind-scaling coefficient used in the TKE model, which must be tuned to simulate data from different locations or climatic regimes.

Turbulence closure models.—The third family of upper-ocean mixing models is the most general, the most complicated, and the most stringently founded in the theoretical and empirical properties of fluid turbulence. These are the "turbulence closure" models, first introduced into the mainstream oceanography literature by Mellor (1973; see also Mellor and Yamada 1974, 1982, Mellor and Durbin 1975). Turbulence closure models were originally constructed for use in the atmospheric boundary layer. In the oceans, Mellor's model is general enough to be applied to special cases like the equator, where the equatorial undercurrent produces regions of extremely high shear, and to a system of estuarine circulation, spanning the benthic boundary layer, the highly stratified shear flow between the saline and fresh waters, and the surface boundary layer (Oey et al. 1985).

Formulation.—The physical foundation for the turbulence closure models begins with the full Reynold's equations for momentum and heat (from Mellor 1973):

$$\frac{\partial U}{\partial t} + U\cdot\nabla U + f \times U = \nabla P - g\beta\Theta + \nu\nabla^2 U \quad (20)$$

and

$$\frac{\partial \Theta}{\partial t} + \nabla\cdot U\Theta = \alpha\nabla^2\Theta, \quad (21)$$

where U is velocity, ∇ is the gradient operator, Θ is temperature, f is the coriolis parameter, P is pressure,

g is the gravitational constant, ν is the molecular viscosity, α is the thermal diffusivity, and β is the thermal expansion coefficient. The equations for the mean flow and temperature can be found by decomposing the total velocity and temperature fields into mean and fluctuating components and averaging:

$$\frac{\partial \overline{U}}{\partial t} + \overline{U}\cdot\nabla\overline{U} + f \times \overline{U} = \nabla\overline{P} - g\beta\overline{\Theta} + \nu\nabla^2\overline{U} - \nabla\cdot\overline{u\,u} \quad (22)$$

and

$$\frac{\partial \overline{\Theta}}{\partial t} + \nabla\cdot\overline{U\Theta} = \alpha\nabla^2\overline{\Theta} - \nabla\cdot\overline{u\,\theta} \quad (23)$$

The terms $\overline{u\,u}$ and $\overline{u\,\theta}$ represent the effect of the turbulent fluctuations on the mean velocity and temperature (the Reynold's stress and "eddy diffusion"). Finding analytical expressions for these terms is the problem at the heart of the turbulence closure models.

Derivation of expressions for these terms begins with these two sets of equations, and incorporates several empirical simplifying relationships based on laboratory data (the interested reader is referred to Mellor [1973]). The salient point to understand about the derivation is that the solutions contain several empirical constants, which are fit to laboratory data from neutral (unstratified) flows. Mellor and Yamada (1982) show the surprising result that the model, using these constants, is also able to predict laboratory data for stratified flow, flow in a pipe, and flow over a curved surface. Some of the terms in the equations also require a constant with units of length to maintain dimensional homogeneity. Mellor assumes that the length scales are all proportional to a single "mixing-length scale" (l). This assumption, and the derivation of a number for l, is considered a weak link in the turbulence closure scheme. The choice of l is crucial; the levels 2 and 2.5 models (see below) supply eddy diffusion coefficients that scale directly to l.

The full version of the model is somewhat cumbersome, and some of the terms can be neglected without loss of predictive value. Mellor and Yamada (1974) present a hierarchy of closure schemes that employ increasing levels of simplification, based on the dependence of each term on the degree of anisotrophy (directional inhomogeneity) of the turbulence (the term is called "a", and is typically $\approx$15% for the ocean surface boundary layer). The level 4 model is simplified the least, and is in general too complicated for routine oceanographic use, without any corresponding benefit in predictive value. The level 3 model neglects all terms that clearly scale with a^2. There is some uncertainty to this scaling procedure. For the level 3 model the advective and diffusive terms for q^2 (a synonym for 2 × TKE) are assumed to scale with a^1 and are left in; for the level 2 model, they are assumed to scale with a^2 and are neglected. This has the important consequence in the level 2 model of setting the diffusive flux of TKE equal to zero, so that all turbulence is dissipated locally to its generation (Niiler and Kraus 1977).

Mellor's model of choice is called the level 2.5 model (Mellor and Yamada 1982). Level 2.5 starts from the level 3 model but neglects the advection and diffusion of variance of the material terms like temperature and salinity (equations for $\overline{\theta^2}$ and $\overline{S^2}$). The result is the elimination of several differential equations; the savings depends on the number of scalar quantities being modeled (e.g., nutrients, pCO_2).

The final, reduced form of the level 2.5 model adds two equations to the averaged equations of motion that would be required to model any geophysical fluid. The first describes the time and space distribution of $q^2/2$, the turbulent kinetic energy. Energy is added at the top as a boundary conditions, advects, and diffuses according to the calculated eddy diffusion coefficient. Turbulent energy is generated by shear at the expense of mean flow. The length scale, l, is determined using a second differential equation for the quantity q^2l. The result of this formulation is that l, the length scale of the largest eddies, is time dependent, has memory, and is allowed to be transported. The eddy diffusion coefficient at a given time and depth is calculated as a function of q^2 and l. Once the diffusion coefficient field is known, it is used for mixing the scalar quantities.

The mixing coefficient predicted by the model turns out to be a function of the local gradient Richardson number (Mellor and Durbin 1975, Niiler and Kraus 1977); above $Ri_{gr} = 0.23$, no mixing at all is predicted. This is similar to the Price model, in which mixing takes place until a critical $Ri_{gr} > 0.25$ is attained. The level 2.5 model has been used in a global ocean model that focuses on the surface ocean and the sea surface temperature (Rosati and Miyakoda 1988).

Behavior.—The turbulence closure models are more difficult to understand in an intuitive way than the other models. Insight can be gained by comparing the behavior of the model with those of the bulk TKE and shear models described above.

One obvious distinction is the degree of mixing in the turbulence closure model mixed layer. Whereas the other formulations assume homogeneity of all properties within the mixed layer, the turbulence models predict high but finite mixing coefficients within this zone. Under conditions of deep convective mixing, the "bulk" assumption (that the mixed layer is completely homogenous in all properties) is probably inadequate, but under conditions of shallower, wind-driven mixing, the "bulk" approximation may be closer to reality than the output of the turbulence models (Martin 1986).

The fundamental distinction between bulk and shear models presented earlier was the source of the turbulent energy for entrainment: from wind stress directly or from current shear, respectively. The main source of entrainment energy in the turbulence closure models is difficult to judge from first principles. For the primary source of turbulence to be generation at the surface,

the rate of transport of turbulent energy through the mixed layer must be greater than the rate of generation of turbulence by shear at the mixed-layer base. In the level 2 model, transport of turbulence does not occur; all turbulence is dissipated locally. Numerical experiments using levels 2.5 and higher models have shown that the transport flux of turbulent energy from the surface zone in these models is also small relative to the generation of turbulence by shear (Klein and Coantic 1981, Martin 1986). Thus the turbulence closure models appear to function primarily as shear instability models.

Mixed-layer model comparison.—All of the models can adequately predict observed fluctuations in the mixed-layer depth in the ocean, under most conditions. There may be situations (for example, the equatorial undercurrent, or regions near a western boundary current) that are more complicated than a mid-gyre mixed layer, and these will probably be better handled by the turbulence closure scheme. On the other hand, simplicity and conservation of computer resources may be the priority, in which case a bulk TKE or shear instability model would be the model of choice.

The stability of empirical parameters.—A criterion for comparison of the model formulations is the quantity and stability of the empirical parameters required for oceanic simulation. The bulk TKE models appear to be weakest in this respect, in that the coefficient that predicts TKE flux into the mixed layer based on the wind stress seems to vary as a function of climatic conditions (see *Integrated TKE, or "bulk", models,* above). The empirical parameters used by the shear instability models are the critical Richardson numbers Ri_b and Ri_{gr}, which do not vary in this way (Price et al. 1978). The constants in the turbulence closure models were determined from laboratory experiments, and appear to be adequate for oceanic use (see Rosati and Miyakoda 1988).

Accuracy.—Detailed comparisons of the ability of each model to simulate oceanic data are presented by Martin (1985, 1986). The latter study is an extension of the former, with the inclusion of the Price et al. (1986) model and a turbulence closure scheme other than Mellor's (Therry and Lacarrere 1983). The conclusions are the following. First, the turbulence closure schemes are essentially Richardson-number-driven models, and the main differences among them (and the Price et al. [1986] model) are the exact value of the critical Richardson number at which mixing commences. Second, the bulk TKE models (as represented by the model of Garwood [1977]) do not attempt to simulate partial mixing at the base of the mixed layer, as do the Price model and the turbulence closure schemes. For this reason, the bulk TKE model mixed-layer base is unrealistic. Third, the turbulence models predict a greater gradient of momentum and density through the mixed layer than is observed (in the data presented in Price et al. [1986]); apparently, some mechanism for mixing exists (such as langmiur circulation) that is not included in the one-dimensional turbulence closure model formulation. Finally, under some circumstances, each of the models predicts mixed-layer depths that deviate somewhat from the observed data.

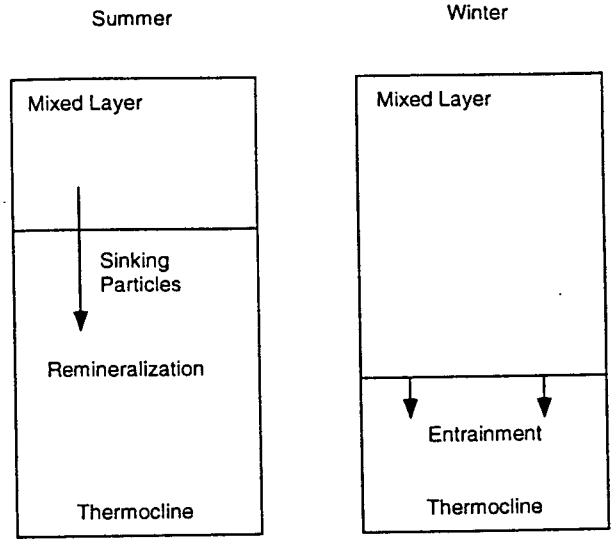

FIG. 7. Schematic diagram of the simplified nutrient cycle in the upper ocean used by Peng et al. (1987).

Computational efficiency.—Martin (1986) also compares the computation time required by the different types of models. As written, the bulk model (Garwood 1977) is the fastest. The Price shear-driven model is significantly slower, mainly because of the calculations involved in maintenance of the partially mixed zone beneath the mixed layer (based on Ri_{gr}; see Eq. 18), which can be eliminated (Archer et al. 1993). The turbulence models are the slowest, because of their complexity and the higher temporal and spatial resolution required. Turbulence models are the most suitable for use in a vectorized or parallel-computer architecture, which would reduce somewhat the computation load disparity between the model types.

Physical transport of dissolved nutrients into the euphotic zone

In addition to light limitation, photosynthesis in the ocean is limited by the availability of dissolved nutrients, primarily nitrate and phosphate (NO_3^- and PO_4^{3-}). Biological production in the surface ocean produces particles that sink into deeper waters, where they ultimately redissolve. This process (called the "biological pump") maintains lower concentrations of nutrients (and CO_2) in the surface ocean than within the thermocline waters below.

A simple model of nutrient cycling in the upper ocean was presented by Peng et al. (1987), to reproduce data from the Greenland sill. The upper box of the model is the mixed layer; the lower box represents the thermocline (Fig. 7). The boundary between the boxes

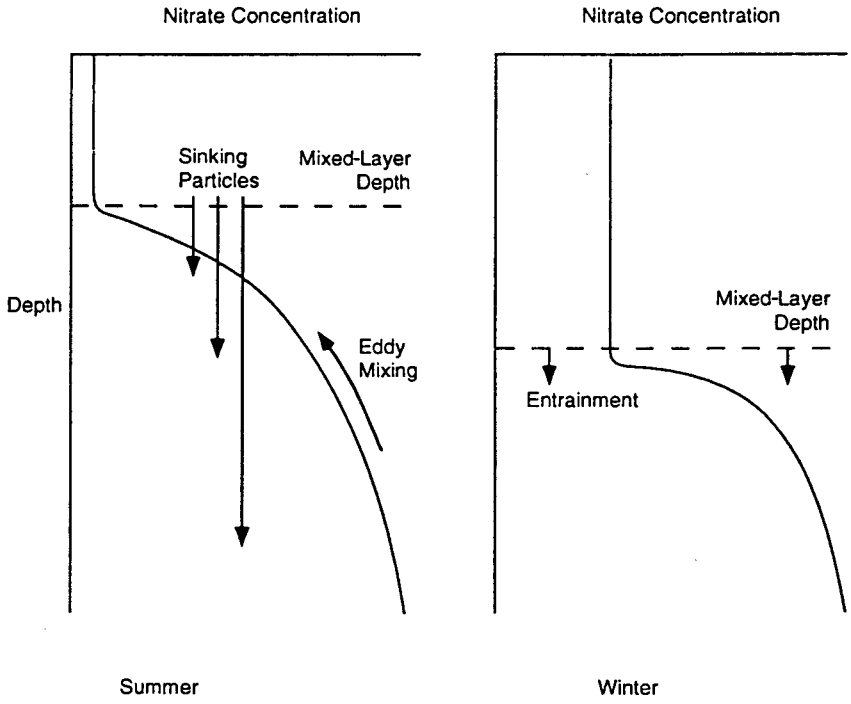

FIG. 8. Diagram of nitrate transport in the upper ocean.

fluctuates according to the observed annual cycle of mixed-layer depth. Both boxes are well-mixed. Organic carbon is produced in the upper box and regenerated within the lower box. When the mixed layer deepens in the winter, nutrients from the deep box are entrained into the mixed layer. The model neglects both the diffusive flux of nutrients across the boundary (either between the two boxes or from the deep ocean into the lower box) and the sinking flux of particles at the bottom boundary. However, the annual cycle of surface water nutrient concentration and the dissolved O_2 and CO_2 predicted by this simple model are similar to the observations.

When the vertical density structure of the water column and the processes of nutrient transport and regeneration are considered in greater detail, the picture becomes more complex (Fig. 8). Although most of the organic matter than falls from the euphotic zone is regenerated in the upper few hundreds of metres of the water column, some fraction ($\approx$25% at 200 m; Martin et al. 1987) inevitably escapes from the deepest reach of the mixed layer; it is this fraction that drives respiration in the deep water and benthos. This loss must be balanced by upward diffusion or advection of nutrients.

In the subpolar gyres, the net upwelling driven by the wind stress curl is an obvious mechanism for transporting nutrients to the euphotic zone. In the subtropical gyres, the net vertical velocity is downward, and accounting for the nutrient supply inferred from the sinking carbon flux is more difficult. Hayward (1987) documented the problem in detail in the central North Pacific, using data from several California–Hawaii transects and quasi-time-series data from a site near Hawaii. The surface nutrient structure in this region is characterized by low nutrient concentrations in the euphotic zone, on top of a "nutricline", or region of nutrient increase with depth. The top of the nutricline is located well below the depth of the seasonal thermocline, and is roughly at the depth of the deepest reach of the mixed layer in winter. No seasonal structure in the nutrient–depth relation was detected in the nutricline data, which would be indicative of entrainment of the nutrient-rich thermocline water into the winter mixed layer. Calculation of nutrient-mixing through the nutricline, based on the paradigm of Fickian eddy mixing, yielded a nutrient supply rate that was an order of magnitude too small to account for the observed production. (This calculation is sensitive to the appropriate value of the eddy mixing coefficient, however, which is not well known.) Perhaps more importantly, Hayward observes that there was no correlation between the nutrient gradient and the productivity rate, as would be predicted by a Fickian eddy-mixing model. He concludes that nutrient supply to the euphotic zone must be more complicated than can be explained by the eddy-mixing formulation. The nutrient supply problem has also been documented in the subtropical Atlantic near Bermuda (Jenkins 1987), with the conclusion that the Fickian "background" eddy-mixing rate is too slow by an order of magnitude to mix nutrients into the euphotic zone fast enough to meet the observed production demand.

Several potential solutions to the nutrient supply

problem have been suggested. Villareal et al. (1993) proposed that diatoms in this region may be able to migrate vertically to reach both the deep nutrients and the shallow euphotic zone in the course of a 24-h cycle. There are also abundant indications that nutrient transport may be an episodic process, rather than a "constant background" eddy diffusive flux. Jenkins (1987) observed an anomalous nutrient profile in the subtropical Atlantic that appeared to represent an injection of high-nutrient thermocline water into the euphotic zone. The apparent transport of nitrate to the euphotic zone during this event was high enough to supply 20–30% of the annual production demand. Based on a calculated residence time of inorganic nitrate, Jenkins calculates that these episodic events could supply the entire nutrient requirement of the euphotic zone, but the probability of actually observing such an event on any given cast would only be ≈1%. Abundant theoretical evidence exists that nutrient transport may be dominated by motions on a frontal- and mesoscale in the upper ocean. Bleck et al. (1988) constructed a two-dimensional, isopycnal, vertical-coordinate, numerical model of a convergent front. Using typical open-ocean conditions, they calculated local time-averaged vertical velocities associated with fronts of >5 m/d. Pollard and Regier (1990) deployed a towed, undulating, CTD (conductivity, temperature, and depth) sensor and an acoustic doppler current profiler in the subtropical Atlantic and inferred that the mechanisms predicted by Bleck et al. (1988) were correct, and that there were vertical velocities of tens of metres per day at that location. Intense fronts are found at the boundaries between water masses (gyres) in the upper ocean; less intense fronts also form during the decay of mesoscale eddies, which are thought to be ubiquitous in the ocean (Semtner and Chervin 1992 and references therein). Strass (1992) presented towed, undulating, vehicle data that included a fluorescence sensor for chlorophyll in addition to CTD measurements. He found the highest values of the subsurface chlorophyll concentration on the anticyclonic side of a front, just as predicted. Also, he found that the spatial scale of chlorophyll variability was similar to the Rossby radius of deformation, as predicted by Woods (1988). The similarity between the spatial scale of chlorophyll patchiness and the physical scale of eddy dynamics (the mesoscale) lends support to the idea that meso- and frontal-scale dynamics control the transport of nutrients to the euphotic zone in the subtropical gyre.

We conclude that while macro-nutrient supply (NO_3 and PO_4) clearly regulates photosynthesis in some pelagic systems, most notably in the subtropical gyres, the mechanisms by which nutrients are supplied to the euphotic zone are still a topic of active research and that an off-the shelf nutrient transport model is as yet not available. In locations such as the subtropical Pacific, where nutrient supply clearly has a dominant role in determining phytoplankton growth and depth distribution (Hayward 1987), a simple eddy diffusion formulation must be used, with the understanding that essential characteristics of nutrient transport, and thus their effect on phytoplankton dynamics, may be missing.

Summary

Ecosystem dynamics in the upper ocean are heavily influenced, if not controlled, by the physics of mixing, both in the surface turbulent layer, and between nutrient-rich deep waters and the depleted waters within the euphotic zone. We have seen that some aspects of the problem of ocean mixing are well understood, while other aspects of the problem are still murky. In particular, several classes of models exist to describe the dynamics of the surface mixed layer. In contrast, the processes by which nutrients are supplied to the euphotic zone (presumably mixing with nutrient-rich subsurface waters) are not well understood.

Acknowledgments

Parts of this document were written with support from the U.S. Department of Energy under contract DE-AC06-76RLO 1830 with the Battelle Memorial Institute, and were distributed as technical report TRO50 (1990).

Literature Cited

Archer, D. E., S. Emerson, T. Powell, and C. S. Wong. 1993. Numerical prediction of pCO_2 at the sea surface at weatherships station Papa. Progress in Oceanography **32**:319–351.

Archer, D. E., and E. Maier-Reimer. 1994. Effect of deep-sea sediment calcite preservation on atmospheric CO_2 concentration. Nature **367**:260–264.

Baumgartner, A., and E. Reichel. 1975. The world water balance: mean annual global, continental and maritime precipitation, evaporation and run-off. Elsevier, Amsterdam, The Netherlands.

Bleck, R., R. Onken, and J. D. Woods. 1988. A two-dimensional model of mesoscale frontogenesis in the ocean. Quarterly Journal of the Royal Meteorological Society **114**: 347–371.

Broecker, W. S. 1991. Keeping global change honest. Global Biogeochemical Cycles **5**:191–192.

Broecker, W. S., and T. H. Peng. 1982. Tracers in the sea. Eldigio Press, Palisades, New York, USA.

Charlson, R., J. E. Lovelock, M. O. Andreae, and S. G. Warren. 1987. Oceanic phytoplankton, atmospheric sulfur, cloud albedo and climate. Nature **326**:655–661.

Chipman, D. W., J. Marra, and T. Takahashi. 1992. Primary production at 47° N and 20° W in the North Atlantic Ocean: a comparison between the ^{14}C incubation method and mixed layer carbon budget observations. Deep-Sea Research **34**: 1229–1243.

Clayton, T. D., and R. H. Byrne. 1993. Calibration of *m*-cresol purple on the total hydrogen ion concentration scale and its application to CO_2-system characteristics. Deep-Sea Research **40**:2115–2129.

Davis, R. E., R. deSzoeke, and P. Niiler. 1981. Variability in the upper ocean during MILE. Part I. The heat and momentum balances. Deep-Sea Research **28**:1427–1451.

Davis, R. E., R. deSzoeke, and P. Niiler. 1981. Variability in the upper ocean during MILE. Part II. Modeling the mixed layer response. Deep-Sea Research **28**:1453–1475.

Dickson, A. G., and F. J. Millero. 1987. A comparison of the equilibrium constants for the dissociation of carbonic acid in seawater media. Deep-Sea Research **34**:1733–1743.

Ellison, T. H., and J. S. Turner. 1959. Turbulent entrainment in stratified flows. Journal of Fluid Mechanics **6**:423–448.

Elsberry, R. L., T. S. Friam, and R. N. J. Trapnell. 1976. A mixed layer model of the oceanic thermal response to hurricanes. Journal of Geophysical Research **81**:1153–1162.

Evans. G. T., and J. S. Parslow. 1985. A model of annual plankton cycles. Biological Oceanography **3**:327–347.

Fenchel, T. 1988. Marine plankton food chains. Annual Review of Ecology and Systematics **19**:19–38.

Frost, B. W. 1987. Grazing control of phytoplankton stock in the open subarctic Pacific Ocean: a model assessing the role of mesozooplankton, particularly the large calanoid copepod *Neocalanus* spp. Marine Ecology Progress Series **39**:49–68.

Frouin, R., D. W. Linger, C. Gautier, K. S. Baker, and R. C. Smith. 1989. A simple analytical formula to compute clear sky total and photosynthetically available solar irradiance at the ocean surface. Journal of Geophysical Research **94**: 9731–9743.

Gargett, A. E., T. B. Sanford, and T. R. Osborn. 1979. Surface mixing layers in the Sargasso Sea. Journal of Physical Oceanography **9**:1090–1111.

Garwood, R. W. 1977. An ocean mixed layer model capable of simulating cyclic states. Journal of Physical Oceanography **7**:455–468.

Gaspar, P. 1988. Modeling the seasonal cycle of the upper ocean. Journal of Physical Oceanography **18**:161–180.

Gill, A. E. 1982. Atmosphere–ocean dynamics. Academic Press, Orlando, Florida, USA.

Hansson, I. 1973. A new set of acidity constants for carbonic acid and boric acid in seawater. Deep-Sea Research **20**: 461–478.

Hayward, T. L. 1987. The nutrient distribution and primary production in the central North Pacific. Deep-Sea Research **34**:1593–1627.

Holm-Hansen, O., E. W. Helbling, and D. Lubin. 1993. Ultraviolet radiation in Antarctica: inhibition of primary production. Photochemistry and Photobiology **58**:567–571.

Jenkins, W. J. 1987. The use of anthropogenic tritium and helium-3 to study subtropical gyre ventilation and circulation. Philosophical Transactions of the Royal Society of London **325**:43–61.

Jerlov, N. G. 1976. Marine optics. Elsevier, Amsterdam, The Netherlands.

Johansson, O., and M. Wedborg. 1982. On the evaluation of potentiometric titrations of seawater with hydrochloric acid. Oceanologica Acta **5**:209–218.

Johnson, K. M., A. E. King, and J. Sieburth. 1985. Coulometric ΣCO_2 analyses for marine studies: an introduction. Marine Chemistry **16**:61–82.

Keller, M. D., W. K. Bellows, and R. R. L. Guillard. 1989. A survey of DMS production in twelve classes of marine phytoplankton. Pages 167–182 *in* E. Saltzman and W. Cooper, editors. Biogenic sulfur in the environment. American Chemical Society, Washington, D.C., USA.

Kim, J.-W. 1976. A generalized bulk model of the oceanic mixed layer. Journal of Physical Oceanography **6**:686–695.

Klein, P., and M. Coantic. 1981. A numerical study of turbulent processes in the marine upper layers. Journal of Physical Oceanography **11**:849–863.

Knox, F., and M. McElroy. 1984. Change in atmospheric CO_2: influence of the marine biota at high latitude. Journal of Geophysical Research **89**:4629–4637.

Kraus, E. B., and J. S. Turner. 1967. A one-dimensional model of the seasonal thermocline. II. The general theory and its consequences. Tellus **19**:98–105.

Lisitzin, A. P. 1967. Basic relationships in distribution of modern siliceous sediments and their connection with climatic zonation. International Geology Review **9**:631–652, 842–863, 1114–1130.

Lorius, C., J. Jouzel, D. Raynaud, J. Hansen, and H. L. Treut. 1991. The ice-core record: climate sensitivity and future greenhouse warming. Nature **347**:139–145.

Martin, J. H., and S. E. Fitzwater. 1988. Iron deficiency limits phytoplankton growth in the north-east Pacific subarctic. Nature **331**:341–343.

Martin, J. H., and R. M. Gordon. 1988. Northeast Pacific iron distributions in relation to phytoplankton productivity. Deep-Sea Research **35**:177–196.

Martin, J. H., G. A. Knauer, D. M. Karl, and W. M. Broenkow. 1987. VERTEX: carbon cycling in the northeast Pacific. Deep-Sea Research **34**:267–285.

Martin, P. J. 1985. Simulation of the mixed layer at OWS November and Papa with several models. Journal of Geophysical Research **90**:903–916.

———. 1986. Testing and comparison of several mixed-layer models. Technical Report Number 143. Naval Research Laboratory, Stennis Space Center, Mississippi, USA.

Mehrbach, C., C. Culberson, J. E. Hawley, and R. M. Pytkowicz. 1973. Measurement of the apparent dissociation constants of carbonic acid in seawater at atmospheric pressure. Limnology and Oceanography **18**:897–907.

Mellor, G. L. 1973. Analytic prediction of the properties of stratified planetary surface layers. Journal of the Atmospheric Sciences **30**:1061–1069.

Mellor, G. L., and P. A. Durbin. 1975. The structure and dynamics of the ocean surface mixed layer. Journal of Physical Oceanography **5**:718–728.

Mellor, G. L., and T. Yamada. 1974. A hierarchy of turbulence closure models for planetary boundary layers. Journal of the Atmospheric Sciences **31**:1791–1806.

Mellor, G. L., and T. Yamada. 1982. Development of a turbulence closure model for geophysical fluid problems. Reviews of Geophysics and Space Physics **20**:851–875.

Miller, C. B., B. W. Frost, P. A. Wheeler, M. R. Landry, N. Welschmeyer, and T. M. Powell. 1991. Ecological dynamics in the subarctic Pacific, a possibly iron-limited ecosystem. Limnology and Oceanography **36**:1600–1615.

Millero, F. J., R. H. Byrne, R. Wanninkhof, R. Feely, T. Clayton, P. Murphy, and M. Lamb. 1993. The internal consistency of CO_2 measurements in the equatorial Pacific. Marine Chemistry **44**:269–280.

Mitchell, J. F. B., C. A. Senior, and J. W. Ingram. 1989. CO_2 and climate: a missing feedback? Nature **341**:132–134.

Morel, A. 1988. Optical modeling of the upper ocean in relation to its biogenous matter content (Case I waters). Journal of Geophysical Research **93**:10749–10768.

Morel, F. M. M., J. G. Reuter, and N. M. Price. 1991. Iron nutrition of phytoplankton. Oceanography **4**:71–78.

Niiler, P. P., and E. B. Kraus. 1977. One-dimensional models of the upper ocean. Pages 143–172 *in* E. B. Kraus, editor. Modelling and prediction of the upper layers of the ocean. Pergamon Press, Oxford, England.

Oey, L.-Y., G. L. Mellor, and R. I. Hires. 1985. A three-dimensional simulation of the Hudson–Raritan estuary. Part I. Description of the model and model simulations. Journal of Physical Oceanography **15**:1676–1692.

Owens, N. J. P., J. N. Galloway, and R. A. Duce. 1992. Episodic atmospheric nitrogen deposition to oligotrophic oceans. Nature **357**:397–399.

Parsons, T. R., M. Takahashi, and B. Hargrave. 1984. Biological oceanographic processes. Pergamon Press, Oxford, England.

Peixoto, J. P., and A. H. Oort. 1983. The atmospheric branch of the hydrological cycle and climate. Pages 5–65 *in* A. Street-Perrott, editor. Variations of the global water budget. Reidel, London, England.

Peixoto, J. P., and A. H. Oort. 1992. Physics of climate. American institute of Physics, New York, New York, USA.

Peng, T.-H., T. Takahashi, W. S. Broecker, and J. Olafsson. 1987. Seasonal variability of carbon dioxide, nutrients, and oxygen in the northern North Atlantic surface water: observations and a model. Tellus **39B**:439–458.

Pollard, R. T., and L. Regier. 1990. Large variations in potential vorticity at small spatial scales in the upper ocean. Nature **348**:227–229.

Pollard, R. T., P. B. Rhines, and R. O. R.Y. Thompson. 1973. The deepening of the wind-mixed layer. Geophysical Fluid Dynamics **3**:381–404.

Price, J. F., C. N. K. Mooers, and L. Van. 1978. Observations and simulation of storm-induced mixed-layer deepening. Journal of Physical Oceanography **8**:582–599.

Price, J. F., R. A. Weller, and R. Pinkle. 1986. Diurnal cycling: observations and models of the upper ocean response to diurnal heating, cooling and wind mixing. Journal of Geophysical Research **91**:8411–8427.

Redfield, A. C. 1934. On the proportions of organic derivatives in sea water and their relation to the composition of plankton. Pages 176–192 *in* James Johnson memorial volume. Liverpool, England.

Reuter, J. G., and D. R. Ades. 1987. The role of iron nutrition in photosynthesis and nitrogen assimilation in *Scenedesmus quandricuada* (Chlorophyceae). Journal of Phycology **23**: 452–457.

Riebesell, U., D. A. Wolf-Gladrow, and V. Smetacek. 1993. Carbon dioxide limitation of marine phytoplankton growth rates. Nature **361**:249–251.

Rosati, A., and K. Miyakoda. 1988. A general circulation model for upper ocean simulation. Journal of Physical Oceanography **18**:1601–1626.

Roy, R. N., L. N. Roy, K. M. Vogel, C. Porter-Moore, T. Pearson, C. E. Goode, W. Davis, F. J. Millero, and D. M. Campbell. 1993. the dissociation constants of carbonic acid in seawater at salinities 5 to 45 and temperatures 0 to 45°C. Marine Chemistry **44**:249–267.

Ryther, J. H. 1969. Photosynthesis and fish production in the sea. Science **166**:72–76.

Sarmiento, J. L., and R. Toggweiler. 1984. A new model for the role of the oceans in determining atmospheric pCO_2. Nature **308**:621–624.

Sathyendranath, S., and T. Platt. 1988. The spectral irradiance field at the surface and in the interior of the ocean: a model for applications in oceanography and remote sensing. Journal of Geophysical Research **93**:9207–9280.

Seager, R., S. E. Zebiak, and M. A. Cane. 1988. A model of the tropical pacific sea surface temperature climatology. Journal of Geophysical Research **93**:1265–1280.

Semtner, A. J., and R. M. Chervin. 1992. Ocean general circulation from a global eddy-resolving model. Journal of Geophysical Research **97**:5493–5551.

Siegenthaler, U., and T. Wenk. 1984. Rapid atmospheric CO_2 variations and ocean circulation. Nature **308**:624–626.

Smith, R. C., B. B. Prezelin, K. S. Baker, R. R. Bidigare, N. P. Boucher, T. Coley, D. Karentz, S. MacIntyre, H. A. Matlich, D. Menzies, M. Ondrusek, and Z. Wan. 1992. Ozone depletion: ultraviolet radiation and phytoplankton biology in Antarctic waters. Science **255**:952–959.

Stevenson, J. W. 1979. On the effect of dissipation on seasonal thermocline models. Journal of Physical Oceanography **9**:57–64.

Strass, V. H. 1992. Chlorophyll patchiness caused by mesoscale upwelling at fronts. Deep-Sea Research **39**:75–96.

Stumm, W., and J. J. Morgan. 1981. Aquatic chemistry. John Wiley & Sons, New York, New York, USA.

Sverdrup, H. U. 1953. On conditions for the vernal blooming of phytoplankton. Journal du Conseil International pour l' Exploration de la Mer **18**:287–295.

Takahashi, T., W. S. Broecker, A. E. Bainbridge, and R. F. Weiss. 1980. Carbonate chemistry of the Atlantic, Pacific, and Indian Oceans: the results of the GEOSECS expeditions, 1972–1978. National Science Foundation, Washington D.C., USA.

Takahashi, T., W. S. Broecker, and S. Langer. 1985. Redfield ratio based on chemical data from isopycnal surfaces. Journal of Geophysical Research **90**:6907–6924.

Takahashi, T., J. Olafsson, J. G. Goddard, D. W. Chipman, and S. C. Sutherland. 1993. Seasonal variation of CO_2 and nutrients in the high-latitude surface oceans: a comparative study. Global Biogeochemical Cycles **7**:843–878.

Therry, G., and P. Lacarrere. 1983. Improving the eddy kinetic energy model for planetary boundary layer description. Boundary-Layer Meteorology **25**:63–88.

Villareal, T. A., M. A. Altabet, and K. Culver-Rymsza. 1993. Nitrogen transport by vertically migrating diatom mats in the North Pacific Ocean. Nature **363**:709–712.

Weare, B. C., P. T. Strub, and M. D. Samuel. 1981. Annual mean surface heat fluxes in the tropical Pacific Ocean. Journal of Physical Oceanography **11**:705–717.

Weiss, R. 1974. Carbon dioxide in water and seawater. The solubility of a non-ideal gas. Marine Chemistry **2**:203–215.

Wigley, T. M. L. 1989. Possible climate change due to SO_2-derived cloud condensation nuclei. Nature **339**:365–367.

Woods, J. 1988. Mesoscale upwelling and primary production. Pages 7–38 *in* B. J. Rothschild, editor. Toward a theory on biological–physical interactions in the world ocean. Kluwer, Amsterdam, The Netherlands.

Woods, J. D., and W. Barkmann. 1986. The response of the upper ocean to solar heating. I. The mixed layer. Quarterly Journal of the Royal Meteorological Society **112**:1–42.

Wu, J. 1982. Wind-stress coefficients over sea surface from breeze to hurricane. Journal of Geophysical Research **87**: 9704–9706.

APPENDIX

A) Values of K'_0, K'_1, K'_2, and K'_B, apparent thermodynamic equilibrium constants, where T = temperature in kelvins; S = salinity in grams per kilogram; activity is denoted by braces, and concentration is denoted by brackets; $H_2CO_2^* = H_2CO_3 + CO_2$ (i.e., the two chemical species are grouped together for analytical purposes); eq = aqueous.

The equilibrium constant for the process

$$pCO_2 = H_2CO_3^*(aq)$$

is given by Weiss (1974) as

$$\ln K'_0 = 93.4517(100/T) - 60.2409 + 23.3585 \ln (T/100) + S\{0.0023517 - 0.023655(T/100) + 0.0047036(T/100)^2\}.$$

For the dissociation of *carbonic acid*, Dickson and Millero (1987) give

$$\log_{10}K'_1 = \{-(6320.18/T - 126.3405 + 19.568 \ln T + (19.894 - 840.39/T - 3.0189 \ln T)S^{(0.5)} + 0.00679S)\}$$

and

$$\log_{10}K'_2 = \{-(5143.69/T - 90.1833 + 14.613 \ln T + (17.176 - 690.59/T - 2.6719 \ln T)S^{(0.5)} + 0.02169S)\}.$$

For *boric acid* (B), Johansson and Wedborg (1982) give

$$\log_{10}K'_B = \{-(1030.5/T + 5.5076 - 0.015469S + 1.5339\cdot10^{-4}S^2)\},$$

where the total borate concentration of seawater can be estimated to be

$$\Sigma B = 4.106\cdot10^{-4}S/35.$$

B) A simple algorithm for calculating pCO_2 (partial pressure of CO_2), given values of alkalinity, ΣCO_2 (i.e., CO_2 + HCO_3^-), and salinity; from Takahashi et al. (1980).

```
TALK = total alkalinity,
       charge concentration 10⁻⁶ mol/kg
ΣCO₂ and ΣB in 10⁻⁶ mol/kg

C1 = K'₁/2.0
C2 = 1.0 - 4.0*K'₂/K'₁
C4 = ΣB * K'_B
AHT = 0.7E-8
DO ICNT = 1, 100
 A = TALK - C4/(K'_B + AHT)
 X = A/TCO2
 AH1 = C1*X * (1.0 - X
   + SQRT(1.0 + C2 * X * (-2.+X)))
 IF(0.5E-4 .GE. ABS(1. - AHT-AH1)) EXIT
 AHT = AH1
ENDDO
pCO2 = A * (AH1/K'₁)/(K'₀ * (1.0+2.0*K'₂/AH1))
```